

Nuclear spectroscopy with the $^{62}\text{Ni}(^7\text{Li}, ^6\text{He})^{63}\text{Cu}$ reaction*

R. L. White and K. W. Kemper

Department of Physics, The Florida State University, Tallahassee, Florida 32306

(Received 24 June 1974)

The levels of ^{63}Cu with $E_x \leq 2.51$ MeV have been studied with the $^{62}\text{Ni}(^7\text{Li}, ^6\text{He})^{63}\text{Cu}$ reaction at $E(^7\text{Li}) = 34$ MeV to test the usefulness of this reaction as a spectroscopic tool. Elastic scattering data were taken for the $^7\text{Li} + ^{62}\text{Ni}$ and $^6\text{Li} + ^{63}\text{Cu}$ systems and optical model parameters were extracted so that finite range distorted-wave Born-approximation (DWBA) calculations could be performed. The DWBA differential cross sections well reproduce the shapes of the data. The absolute spectroscopic factors are in excellent over-all agreement with previously published light-ion studies, indicating that the extracted ^6Li optical parameters are a reasonable approximation for the ^6He optical parameters and that the $^7\text{Li} \rightarrow ^6\text{He} + p$ spectroscopic factor is in good agreement with the theoretical value of Cohen and Kurath. In addition, this reaction permits a clear distinction between $p_{3/2}$ and $p_{1/2}$ final-state configurations when very forward angle data are taken.

NUCLEAR REACTIONS $^{62}\text{Ni}(^7\text{Li}, ^6\text{He})$, $(^7\text{Li}, ^7\text{Li})$ $E = 34.0$ MeV; measured $\sigma(\theta)$; deduced optical model parameters; deduced S , from finite range DWBA analysis. $^{63}\text{Cu}(^6\text{Li}, ^6\text{Li})$ $E = 28.1, 30.1, 32.1$ MeV; measured $\sigma(\theta)$; deduced optical model parameters.

I. INTRODUCTION

Single-nucleon transfer reactions with light-ion ($A \leq 4$) projectiles have been used extensively to examine the structure of nuclear levels. In recent years, heavy-ion-induced single-nucleon stripping reactions have been the subject of increased study in an attempt to extract spectroscopic information complimentary to that obtained from the light-ion efforts. Almost all heavy-ion studies have been done with ^{16}O , ^{14}N and, ^{12}C projectiles. Poor energy resolution has limited most of these studies to just a few states in the residual nucleus or to residual nuclei where the level spacing is large. When ^7Li is used as the projectile the experimental difficulties diminish while the theoretically interesting p -state motion between the transferred proton and its core in the projectile is retained; this motion provides a true test of the ability of the finite range distorted-wave Born-approximation (DWBA) theory to reproduce spectroscopic factors as well as the correct shape of the angular distributions.

Only a small amount of published work has dealt with lithium induced single-nucleon transfer reactions.¹⁻⁴ For several targets in the p -shell and the lower half of the s - d shell, Schumacher *et al.*³ have shown that the angular dependence of the differential cross sections as well as the spectroscopic factors for lithium induced single-nucleon transfer reactions are reasonably well reproduced by finite range DWBA calculations. However, because of the well-known difficulties encountered in light-ion studies in this mass

region, sufficient anomalies are present so that a rigorous test of the DWBA was not possible.

The present work describes the results of an investigation of the $^{62}\text{Ni}(^7\text{Li}, ^6\text{He})^{63}\text{Cu}$ reaction. The target nucleus ^{62}Ni was chosen for two reasons: (1) The ($^{16}\text{O}, ^{15}\text{N}$) and ($^{12}\text{C}, ^{11}\text{B}$) reactions have been performed on this target⁵ and some difficulties were encountered in explaining the relative spectroscopic factors.^{5,6} (2) There have been several light-ion proton transfer reactions performed on ^{62}Ni with which a comparison of spectroscopic factors may be made.⁷⁻¹⁰ In the experimental results presented here, angular distributions measured for eight levels were analyzed using the exact finite range DWBA theory. Since no lithium elastic scattering has been reported on targets of mass larger than 40, it was necessary to measure the $^{62}\text{Ni}(^7\text{Li}, ^7\text{Li})^{62}\text{Ni}$ reaction. In addition, the $^{63}\text{Cu}(^6\text{Li}, ^6\text{Li})^{63}\text{Cu}$ reaction was also performed to get optical model parameters which approximate the exit channel ^6He elastic scattering.

II. EXPERIMENTAL PROCEDURE

The ^6Li and ^7Li projectiles used in these experiments were accelerated by the Florida State University super FN tandem Van de Graaff accelerator. The $^6\text{Li}^-$ and $^7\text{Li}^-$ beams were produced by a Heinicke direct radial extraction negative ion source.¹¹ Maximum beam currents during these experiments were 350 nA of Li^{++} on target, but the average current was about 150 nA. The ^{62}Ni and ^{63}Cu targets were made by conventional vacuum evaporation techniques. The ^{62}Ni (98.75%

enriched) was evaporated onto thin ($\sim 10 \mu\text{g}/\text{cm}^2$) carbon foils while the ^{63}Cu was evaporated onto a glass slide coated with NaCl as a release agent, and made into self-supporting targets. The thicknesses of both types of targets were found to be $80\text{--}100 \mu\text{g}/\text{cm}^2$.

Reaction products were detected with a ΔE - E solid state counter telescope. After amplification and appropriate gating, the energy signals were digitized and collected pairwise (ΔE and E) through a CAMAC interface by an EMR-6130 on-line computer. At the end of each run, the events were displayed in a two dimensional array (ΔE vs E) on a storage scope, gates were drawn around each particle type of interest, and the events were sorted by particle type into linear energy spectra ($\Delta E + E$).

A. $^{62}\text{Ni}(^7\text{Li}, ^6\text{He})^{63}\text{Cu}$ reaction

The majority of the data for the $^{62}\text{Ni}(^7\text{Li}, ^6\text{He})^{63}\text{Cu}$ reaction was taken in a quadrupole spectrometer¹² (QD0) which allowed measurements to be made at very small angles. A typical spectrum is shown in Fig. 1. The angular acceptance of the QD0 was limited to $\Delta\theta = 1.5^\circ$ for $\theta > 5^\circ$ and $\Delta\theta = 1.0^\circ$ for $\theta \leq 5^\circ$. For scattering angles greater than 5° the data was taken so that when the QD0 was set to pass the $^6\text{He}^{++}$ ions corresponding to a 1.5 MeV excitation energy in ^{63}Cu , the "flat" part of the momentum band-pass curve easily encompassed

excitation energies from 0.0 to 2.5 MeV. The exact shape of the band-pass curve was determined by comparing the relative peak intensities of two spectra taken at $\theta = 20^\circ$, one of which was taken in a large general purpose scattering chamber (LGPSC)¹³ and used as the calibration standard. For angles less than 5° the collimation was reduced in size to approximate the beam spot of the focused $^6\text{He}^{++}$ particles. This procedure minimizes the relative number of unwanted $^7\text{Li}^{++}$ ions but it also reduces the width of the flat region of the band-pass curve, which was then recalibrated.

Angular distributions were measured for $E(^7\text{Li}) = 34 \text{ MeV}$ at lab angles of $1^\circ, 2.5^\circ\text{--}30.0^\circ$ in 2.5° steps, 35 and 40° for the first three states in ^{63}Cu . Angular distributions for five other states of ^{63}Cu were extracted for $\theta \leq 30^\circ$. To estimate the importance of nondirect nuclear processes, a data point was also taken at $\theta = 165^\circ$. A calibrated pulser was used to identify the energy region of interest and to confirm that the electronics were properly adjusted to view this energy region. No events were observed for $1500 \mu\text{C}$ accumulated charge placing an upper limit of $1 \mu\text{b}/\text{sr}$ on the cross section at $\theta = 165^\circ$. In addition, several forward angles were measured at $E(^7\text{Li}) = 36 \text{ MeV}$. The cross sections at 36 MeV were within 15% of those measured at 34 MeV , giving further confirmation of the direct nature of the $(^7\text{Li}, ^6\text{He})$ reaction in this energy range. A fixed monitor counter was used for the relative normalization

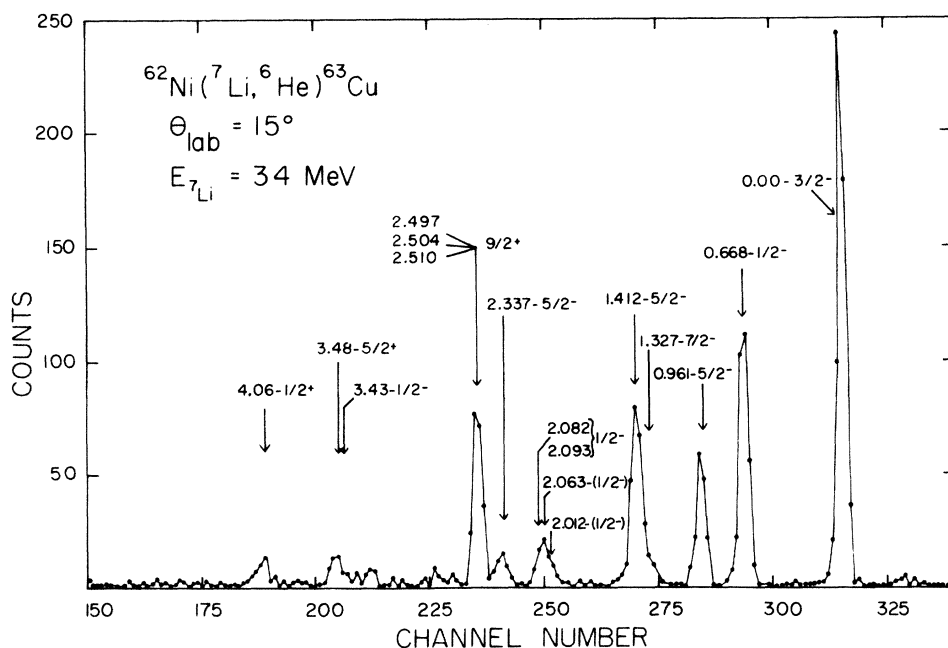


FIG. 1. Sample spectrum from the $^{62}\text{Ni}(^7\text{Li}, ^6\text{He})^{63}\text{Cu}$ reaction taken in the QD0 with the focus set for $E_x = 1.5 \text{ MeV}$ in ^{63}Cu .

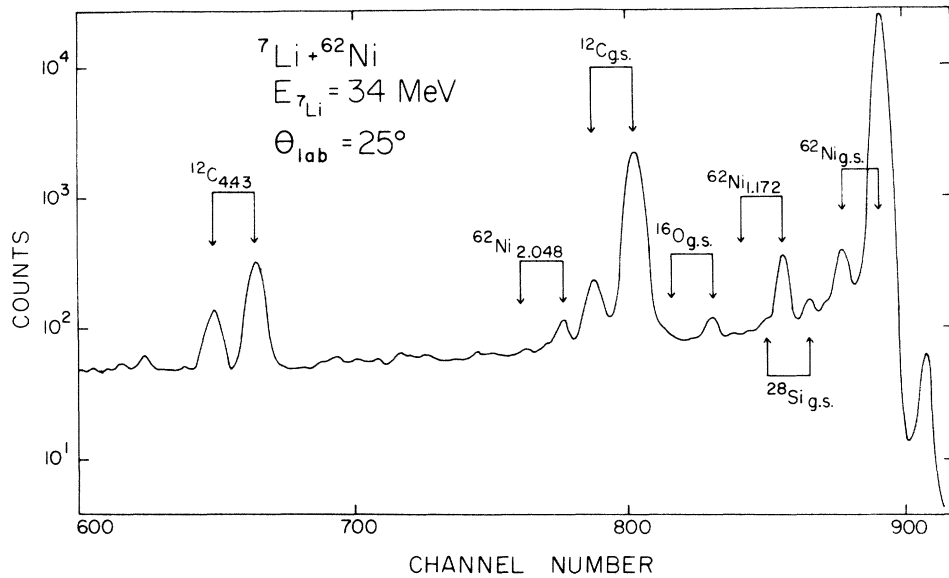


FIG. 2. Sample spectrum of the $^{62}\text{Ni}(^7\text{Li}, ^7\text{Li})^{62}\text{Ni}$ reaction. The double arrow indicates the peak positions when the ^7Li is detected in its ground and first excited state (0.478 MeV) and the target is left in the state indicated above the arrow.

of the various runs. The product of the solid angle and number of target nuclei ($Nd\Omega$) was found by 6 MeV α particle scattering which was taken at $\theta = 25, 30, 35,$ and 40° and was shown to be Rutherford to at least 40° . With this product, the absolute cross sections for the $^{62}\text{Ni}(^7\text{Li}, ^6\text{He})^{63}\text{Cu}$ reaction were calculated.

B. $^{62}\text{Ni}(^7\text{Li}, ^7\text{Li})^{62}\text{Ni}$ and $^{63}\text{Cu}(^6\text{Li}, ^6\text{Li})^{63}\text{Cu}$ reactions

To obtain the best possible estimates for the elastic scattering wave functions, the reactions $^{62}\text{Ni}(^7\text{Li}, ^7\text{Li})^{62}\text{Ni}$ at $E(^7\text{Li}) = 34$ MeV and $^{63}\text{Cu}(^6\text{Li}, ^6\text{Li})^{63}\text{Cu}$ at $E(^6\text{Li}) = 28.1, 30.1,$ and 32.1 MeV were performed. A typical ^7Li spectrum is shown in Fig. 2. ^6Li was chosen for the measurement on ^{63}Cu because the instability of ^6He (β^- ; $T_{1/2} = 0.81$ sec) makes its use as a primary beam impossible. The energy range chosen corresponds to typical outgoing ^6He energies. The scattering was done in

the LGPSC mentioned previously. The data were taken at two angles simultaneously for $\theta = 10^\circ - 25^\circ$ in 2.5° increments and for $\theta = 25^\circ - 75^\circ$ in 5° increments. Particle identification techniques were used for $\theta > 25^\circ$ because of the rapidly decreasing cross section. Absolute normalization was done by the method described in Sec. A. Data for the inelastic excitation of the $^{62}\text{Ni}(2^+)$ were not extracted because of contaminant peaks and its small cross section.

C. Errors

The relative errors in the cross sections are represented by the error bars on the individual data points. In the cases where no error bars are visible, the dot size either equals or exceeds the relative error associated with that point.

For the elastic scattering angular distributions, the error in the absolute scale of the cross section is due to the uncertainty in the deviation from Rutherford scattering at small angles and it is estimated to be $\pm 5\%$. Based on the reproducibility of the ($^7\text{Li}, ^6\text{He}$) data and the consistency of the separate $Nd\Omega$ measurements, the absolute cross sections of the transfer reaction are accurate to $\pm 15\%$.

TABLE I. Optical model parameters.

	U (MeV)	r_R (fm)	a_r (fm)	W (MeV)	r_I (fm)	a_I (fm)
$^7\text{Li} + ^{62}\text{Ni}$						
34.0 MeV	49.7	1.20	0.58	8.5	1.20	1.01
$^6\text{Li} + ^{63}\text{Cu}$						
28.1 MeV	44.2	1.20	0.58	11.8	1.15	0.90
30.1 MeV	47.4	1.20	0.58	11.6	1.15	0.90
32.1 MeV	54.8	1.20	0.58	9.4	1.15	0.90

III. OPTICAL MODEL ANALYSIS

The optical model calculations were performed using the standard potential:

$$V_{\text{opt}}(r) = V_C(r) - Uf(r_R) - iWf(r_I)$$

with the Woods-Saxon form factors

$$f(r_x) = [1 - \exp(r - R_x/a_x)]^{-1}$$

for both the real and imaginary geometries. The first term represents the Coulomb interaction between a point projectile charge and the field of a uniformly charged sphere of radius R_C . The radii in the above expressions are defined to be of the form

$$R_x = r_x (A_T^{1/3} + A_P^{1/3}),$$

in which A_T and A_P are the masses of the target and projectile, respectively, and r_x is an adjustable parameter. All optical model grids and parameter searches were performed with the code JIB3.¹⁴

The question of whether a volume or surface form factor should be used to describe the absorption for lithium scattering has not been answered. In fact, other optical model studies of lithium elastic scattering have indicated that equally good fits can be obtained with either imaginary well

shape.^{15,16} The Woods-Saxon shape was chosen for the absorptive form factor in this work so that the real and imaginary potentials could easily be compared.

The first step in the optical model parametrization was the calculation of χ^2 contours over the U, W surface. In all calculations of χ^2 , the actual errors were used whenever they exceeded the average relative error of 5%; otherwise, 5% was used. The real well depth U was varied in steps of 10 MeV from 10 to 250 MeV and the imaginary well depth W was varied in steps of 5 MeV from 5 to 50 MeV. The geometrical parameters were varied as follows: a_R and a_I were separately varied from 0.6 fm to 1.2 fm in 0.2 fm steps and r_I was varied between 1.0 fm and 2.4 in 0.3 fm steps. The real and Coulomb radii were fixed at $r_R = r_C = 1.2$ fm because of the continuous relationship between U and r_R , $Ur_R = \text{constant}$,^{3,17,18} and the insensitivity of the calculations to small variations of R_C . A χ^2 grid over U and W was

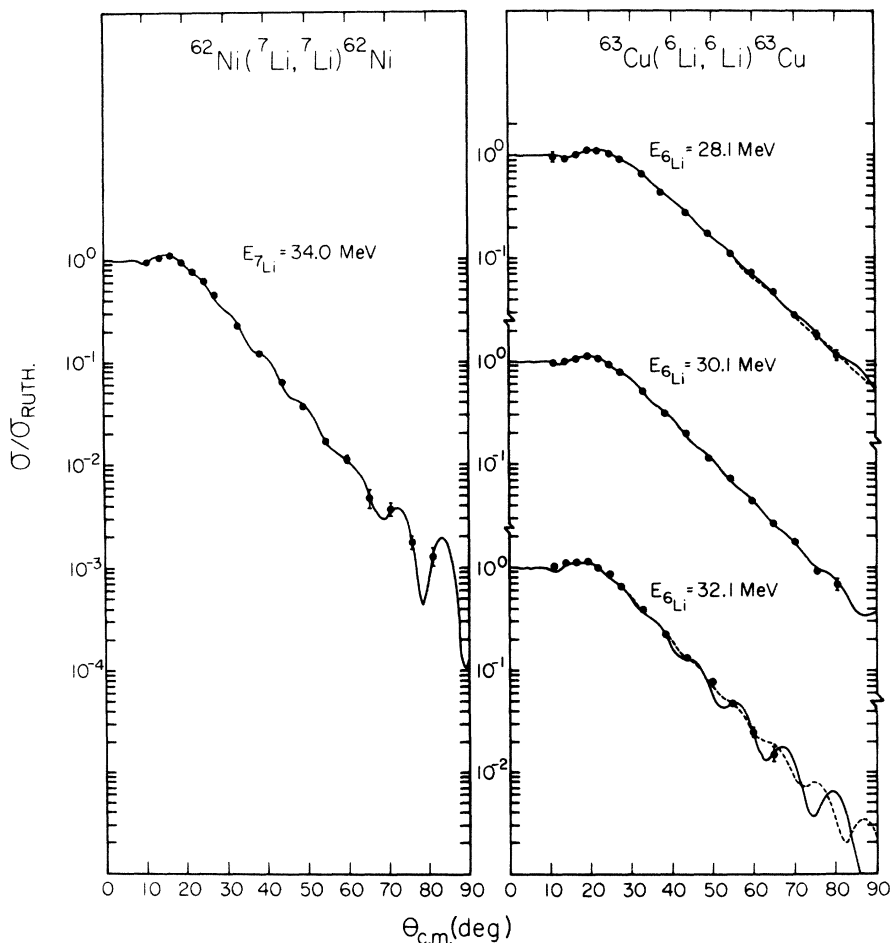


FIG. 3. Elastic scattering angular distributions. The solid lines are best fit optical model calculations. The dashed lines are calculations with the average optical model parameter set used in the DWBA calculations.

performed for each combination of values of a_R , r_I , and a_I .

In contrast to studies of elastic scattering of lithium nuclei on lighter targets¹⁵⁻¹⁸, no discrete ambiguities were found in the present work in either the ${}^7\text{Li} + {}^{62}\text{Ni}$ or the ${}^6\text{Li} + {}^{63}\text{Cu}$ systems. No continuous ambiguities, such as Igo's criterion,¹⁹ were investigated. Direct searches were done around each of the minima found in the grid calculations. In each of the four data sets, one set of potential parameters gave a much smaller value of χ^2 than any other final set.

Since a_R , a_I , and r_I were very similar in all three cases for ${}^6\text{Li} + {}^{63}\text{Cu}$, an average value was taken for these parameters. Then, searches were again performed on U and W to obtain final "best fit" values. These final optical model parameters are shown in Table I, and the best fit parameter curves are shown in Fig. 3 as the solid lines.

To study the sensitivity of the fits to the magnitudes of potential well depth, the parameters obtained from the fit to the 30.1 MeV data were used to calculate cross sections at 28.1 and 32.1 MeV and are shown in Fig. 3 as the dotted curves. It can be seen that the curves fit the data extremely well with the exception of the one point at about 65° in the 32.1 MeV data. Thus, no energy dependence for the potential depths can be extracted. The parameters found from the 30.1 MeV data were used in the subsequent DWBA calculations.

IV. DWBA ANALYSIS

The DWBA analysis of the data from the ${}^{62}\text{Ni}({}^7\text{Li}, {}^6\text{He}){}^{63}\text{Cu}$ reaction was performed with the exact finite range computer code MERCURY.²⁰ The wave functions of the bound proton were generated with Woods-Saxon potentials whose depths were adjusted to give the correct binding energies. The ground state binding energies are -9.980 MeV for $p + {}^6\text{He}$ and -6.124 MeV for $p + {}^{62}\text{Ni}$. The shape parameters were fixed at $r_0 = 1.25$ fm and $a = 0.65$ fm and a spin-orbit strength of $\lambda = 25$ was used in all bound state calculations. No spin-orbit potential was used in the distorted waves.

A. p states

Shown in Fig. 4 are the states of $l = 1$ character along with the calculated DWBA curves. The solid lines are the calculated DWBA differential cross sections while the broken lines are the individual L contributions to that cross section. These partial cross sections may be examined because of the factorization which occurs when no spin-orbit interaction is introduced into the distorted waves. From $({}^3\text{He}, d)$ studies the $E_x = 0.00$ MeV and $E_x = 0.67$ MeV levels have been found to be predominantly single particle states of $2p_{3/2}$ and $2p_{1/2}$ configuration, respectively.^{7,8} At very forward

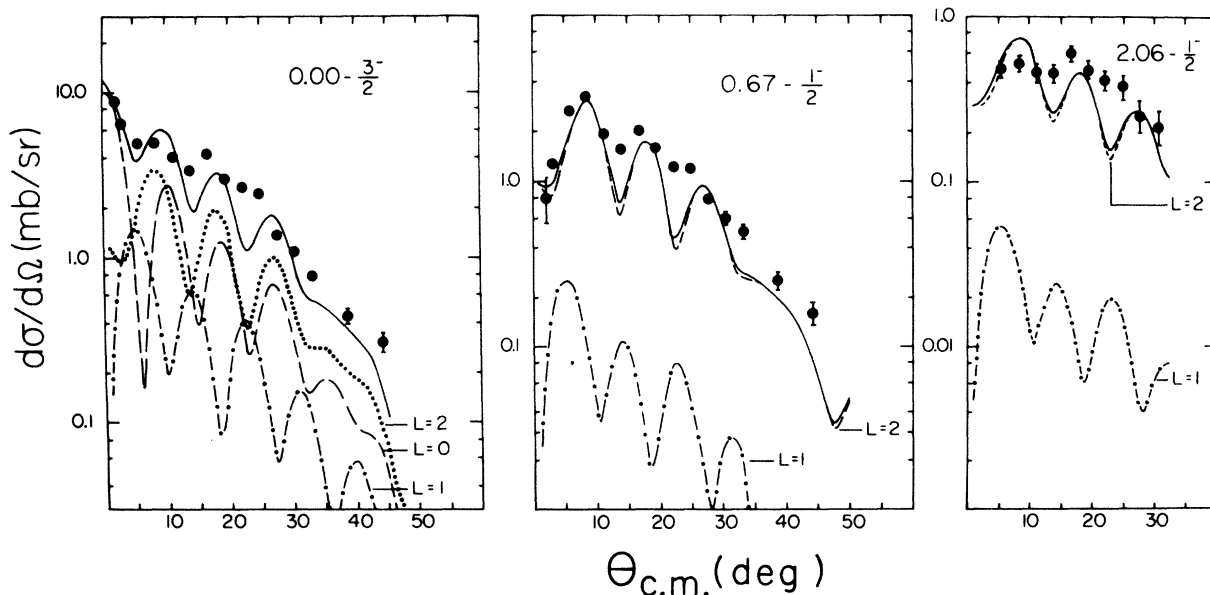


FIG. 4. ${}^6\text{He}$ angular distributions for the ${}^{62}\text{Ni}({}^7\text{Li}, {}^6\text{He}){}^{63}\text{Cu}$ reaction at $E({}^7\text{Li}) = 34.0$ MeV for transitions to states with $l = 1$ character. The solid lines are the DWBA calculations while the broken lines are the L dependent components of those calculations.

angles ($\theta \leq 5^\circ$) these two states exhibit markedly different behavior. The $2p_{3/2}$ cross section is rising while the $2p_{1/2}$ state is falling. These features are well explained by the calculations and have been shown to be a consequence of the selection rules.⁴ For the $2p_{1/2}$ state only $L=1$ and $L=2$ transfers are allowed while the $2p_{3/2}$ state can proceed by $L=0, 1, 2$. The $L=0$ transfer can be seen in Fig. 4 to be the reason for the difference at small angles. The over-all fits to these two levels are very good considering the complexity of the calculations and that no parameters were adjusted to enhance the fit. However, the calculations are more highly structured than the data.

The level at $E_x = 2.06$ MeV is actually a group of four levels of energies, $E_x = 2.012, 2.063, 2.082,$ and 2.093 MeV. In the work of Smith, Chen, and Enge⁸ it was shown that the 2.012 MeV level is definitely excited with approximately one-third the intensity of the other three states as a group. All four states have been assumed to be $2p_{1/2}$ levels for the purpose of (${}^3\text{He}, d$) DWBA calcula-

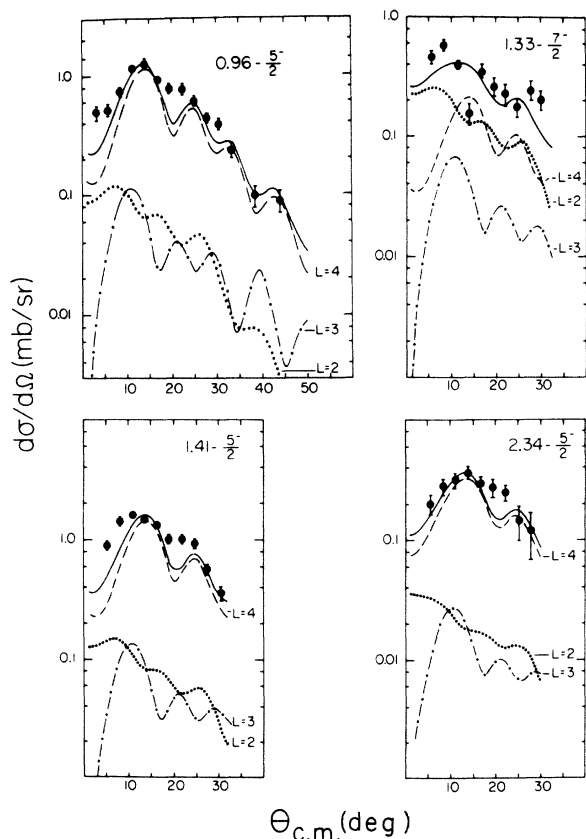


FIG. 5. ${}^6\text{He}$ angular distributions for transitions to levels with $l=3$ character. The solid lines are the DWBA calculations while the broken lines are the L dependent components of those calculations.

tions, and this was also assumed here. The calculation and data are also shown in Fig. 4. The poor fit may indicate that one of the stronger levels in the clump is not of $2p_{1/2}$ structure.

B. f states

The states shown in Fig. 5 have been assumed to be $l=3$ states for the DWBA calculations. The levels at $E_x = 0.96$ and 2.34 MeV are fitted extremely well by the DWBA calculations. The underestimation of the cross section around the minima is the only drawback of the calculations. The fit to the level at $E_x = 1.41$ MeV is reasonable although the main stripping peak in the data is 2 or 3° wider than the calculation. For the three $\frac{5}{2}^-$ states just discussed, the DWBA predictions are almost entirely due to the $L=4$ transfer, and so are quite oscillatory and have very steeply rising cross sections from 0° to about 14° (a factor of 5 to 10). Also shown in Fig. 5 is the data for the $\frac{7}{2}^-$ level at $E_x = 1.33$ MeV along with a DWBA calculation which assumes a $1f_{7/2}$ configuration. This configuration was assumed in the (${}^3\text{He}, d$) work and was used here for comparative purposes.

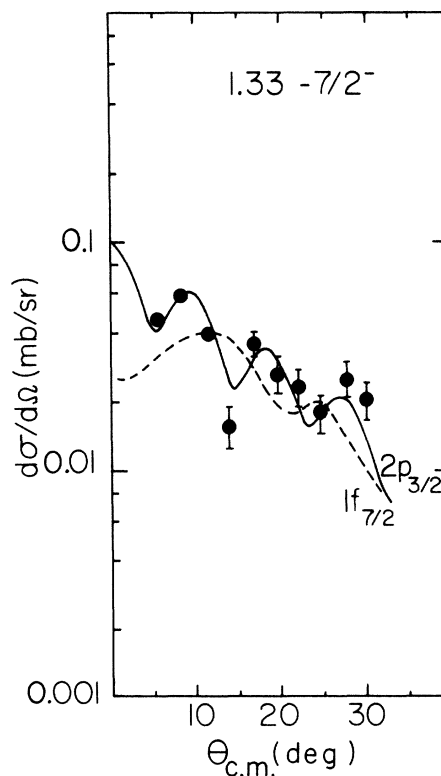


FIG. 6. DWBA calculation for the $E_x = 1.33$ MeV, $\frac{7}{2}^-$ level assuming the state is made by transfer into a $2p_{3/2}$ orbit which is coupled to ${}^{62}\text{Ni}(2^+)$.

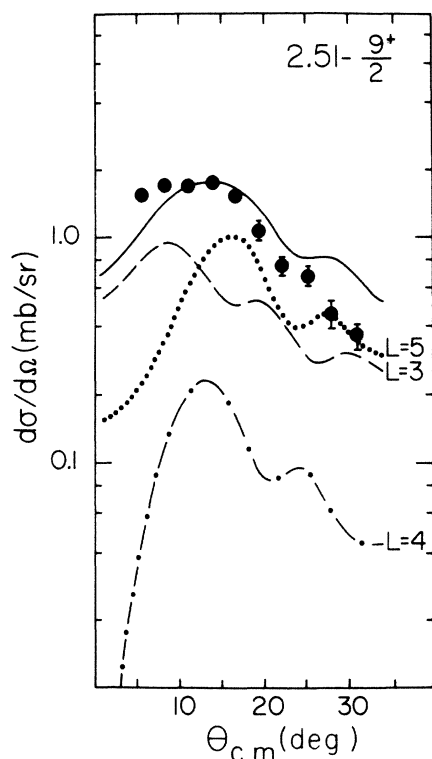


FIG. 7. ${}^6\text{He}$ angular distribution of the transition to the $l=4$ level $E_x=2.51$ MeV. The solid line is the DWBA calculation while the broken lines are the L dependent components of the calculation.

It is seen that since the $L=2$ component is almost a factor of 11 stronger, relatively, than in the $\frac{5}{2}^-$ cases, the oscillatory features are damped and the cross section is much flatter between 0 and 14° . The makeup of the $E_x=1.33$ MeV state is predicted theoretically to be predominantly a

$2p_{3/2}$ proton coupled to the 2^+ state of ${}^{62}\text{Ni}$.^{21,22} In the absence of any $1f_{7/2}$ hole component in the ${}^{62}\text{Ni}$ ground state, the state can be reached only through a secondary reaction which would account for the poor fit to the data. As pure speculation, a $2p_{3/2}$ calculation for the appropriate bound state was performed and is shown in Fig. 6 with the data for the $E_x=1.33$ MeV level. From the population of this level some conclusions may be drawn: (1) The state does not have an $l=3$ shape and therefore is not due to a $1f_{7/2}$ hole component in ${}^{62}\text{Ni}$. (2) Two-step contributions may not be negligible in (${}^7\text{Li}$, ${}^6\text{He}$) reactions.

C. g state

The level $E_x=2.51$ MeV shown in Fig. 7 is known to be a $\frac{9}{2}^+$. But, as is shown in the typical spectrum, Fig. 1, there are two "contaminant" levels of energies $E_x=2.497$ MeV and $E_x=2.504$ MeV in the extracted data group. For this reason, the $1g_{9/2}$ DWBA calculation might not be expected to reproduce the data, and such is the case. The general trend of the data is reproduced as well as it is in the two (${}^3\text{He}$, d) studies referenced earlier.

D. Spectroscopic factors

The experimental cross section is related to the calculated cross section by

$$\frac{d\sigma}{d\Omega}(\theta)_{\text{exp}} = (C^2S)_{7\text{Li}} (C^2S)_{63\text{Cu}} \frac{d\sigma}{d\Omega}(\theta)_{\text{merc}}$$

where the S 's are spectroscopic factors and the C 's are the relevant isospin Clebsch-Gordan coefficients. Therefore, by normalizing the calculations to the experimental data, the product of the spectroscopic factors may be obtained. The value

TABLE II. Spectroscopic factors of the low lying ${}^{63}\text{Cu}$ levels.

Level (MeV)	$J\pi$	$({}^3\text{He}, d)^a$	Measured spectroscopic factors (C^2S)			
			$({}^3\text{He}, d)^b$	$({}^4\text{He}, t)^c$	$(d, n)^d$	$({}^7\text{Li}, {}^6\text{He})^e$
0.00	$\frac{3}{2}^-$	0.66	0.78	0.56	0.61	0.60
0.67	$\frac{1}{2}^-$	0.70	0.71	0.76	0.78	0.71
0.96	$\frac{5}{2}^-$	0.33	0.29	0.46	...	0.46
1.33	$\frac{7}{2}^-$	0.057	0.072	0.10	...	0.10
1.41	$\frac{5}{2}^-$	0.45	0.34	0.68	0.83	0.58
2.06	$\frac{1}{2}^-$	0.23	0.195	...	0.29	0.30
2.35	$\frac{5}{2}^-$	0.10	0.53	0.13
2.51	$\frac{9}{2}^+$	0.31	...	0.28	...	0.52

^a Reference 7.

^b Reference 8.

^c Reference 9.

^d Reference 10.

^e This work.

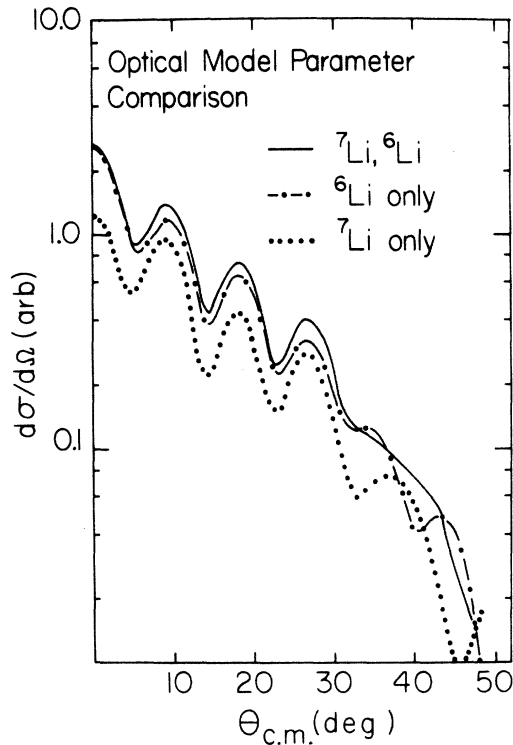


FIG. 8. Three DWBA calculations showing the effect of using the same optical model parameters for both the entrance and exit channels.

for $S_{7\text{Li}} = (0.8884)$ was taken from Cohen and Kurath²³ and the value for $(C^2S)_{7\text{Li}}$ is then 0.59. Using this value, the $(C^2S)_{63\text{Cu}}$ was extracted for each level and they are tabulated in Table II along with values obtained from other reactions. The $(^7\text{Li}, ^6\text{He})$ reaction is shown to give absolute spectroscopic factors in excellent agreement with those from the light-ion reactions.

To investigate the sensitivity of the spectroscopic factors to entrance and exit channel optical model parameter sets, calculations were performed for the ground state transition using the same parameters for both channels. For heavier-ion reactions, this technique has been used frequently. The results of the calculations for the ground state transition are shown in Fig. 8. The calculation, using only the ^6Li parameters, yields spectroscopic factors close to those of the actual calculation while the calculation with the ^7Li parameters only gives spectroscopic factors approximately 60–100% larger. This points out that even when there are only small differences in the two potential sets, large discrepancies in the absolute spectroscopic factors may result. Therefore, it is a very

dubious practice to use only a single optical parameter set in DWBA calculations.

V. CONCLUSIONS

The elastic scattering of ^7Li by ^{62}Ni at 34 MeV and of ^6Li by ^{63}Cu at 28.1, 30.1, and 32.1 MeV is well described by the standard optical model. No discrete ambiguities of potential parameter families were observed. Also, no energy dependence in the optical parameters was observed in the 4 MeV range studied for the $^6\text{Li} + ^{63}\text{Cu}$ system.

The compound nuclear contribution to the $^{62}\text{Ni}(^7\text{Li}, ^6\text{He})^{63}\text{Cu}$ reaction was shown to be negligible by taking forward angle data at 34 and 36 MeV, as well as a data point at 165° . The shape of the angular distribution to the 1.33 MeV state shows that this state is not predominantly of $f_{7/2}$ character. If the theoretical interpretation of this state as $^{62}\text{Ni}(2^+) \otimes p_{3/2}$ is correct then the population of this state means that two-step contributions are possible in the $(^7\text{Li}, ^6\text{He})$ reaction.

The calculated DWBA cross sections and, therefore, the deduced spectroscopic factors are from a single calculation for each level. The use of the same set of optical parameters in both the entrance and exit channels has been shown to lead to spectroscopic factors which can vary by 100% from those obtained with the appropriate potentials. The agreement of shape and magnitude between the data and the theory illustrates that to a high degree the ^6He optical potential can be approximated by the ^6Li optical potential.

The absolute spectroscopic factors, shown in Table II, are in excellent over-all agreement with all published values, indicating that the spectroscopic factor for $(^7\text{Li} \rightarrow ^6\text{He} + p)$ as calculated by Cohen and Kurath²³ is consistent with experimental results. This work has shown that the $(^7\text{Li}, ^6\text{He})$ reaction can give important final state spin information as well as reliable spectroscopic factors, which should make it an important spectroscopic tool.

ACKNOWLEDGMENTS

The authors would like to acknowledge the assistance during the data taking of G. Gunn, M. Hudson, G. Moore, G. Norton, R. Puigh, and M. Williams. The invaluable help of G. Kiess in the data reduction is gratefully acknowledged, and the assistance of L. Charlton in the theoretical calculations is much appreciated. We also wish to thank D. Robson and other members of the Florida State University nuclear physics group for their many encouraging discussions.

- *Work supported in part by the National Science Foundation grants Nos. NSF-GU-2612, NSF-GP-25974, and NSF-GJ-367.
- ¹K. O. Groeneveld, A. Richter, U. Strobbusch, and B. Zeidman, *Phys. Rev. Lett.* **27**, 1806 (1971).
- ²K. I. Kubo, H. H. Duhm, and N. Ueta, *Phys. Lett.* **45B**, 299 (1973).
- ³P. Schumacher, N. Ueta, H. H. Duhm, K. I. Kubo, and W. J. Klages, *Nucl. Phys.* **A212**, 573 (1973).
- ⁴R. L. White, K. W. Kemper, L. A. Charlton, and G. D. Gunn, *Phys. Rev. Lett.* **32**, 892 (1974).
- ⁵D. G. Kovar, F. D. Becchetti, B. G. Harvey, F. Pühlhofer, J. Mahoney, D. W. Miller, and M. S. Zisman, *Phys. Rev. Lett.* **29**, 1023 (1972).
- ⁶L. A. Charlton, *Phys. Rev. Lett.* **31**, 116 (1973).
- ⁷A. G. Blair, *Phys. Rev.* **140**, B648 (1965).
- ⁸D. L. Smith, H. Y. Chen, and H. A. Enge, *Nucl. Phys.* **A107**, 639 (1968).
- ⁹D. D. Armstrong, A. G. Blair, and H. C. Thomas, *Phys. Rev.* **155**, 1254 (1967).
- ¹⁰V. V. Okorokov *et al.*, *Yad. Fiz.* **8**, 668 (1968) [transl.: *Sov. J. Nucl. Phys.* **8**, 387 (1969)].
- ¹¹E. Heinicke, K. Bethge, and H. Baumann, *Nucl. Instrum. Methods* **58**, 125 (1968); E. Heinicke and H. Baumann, *ibid.* **74**, 229 (1969).
- ¹²G. R. Morgan, G. D. Gunn, N. R. Fletcher, J. D. Fox, M. B. Greenfield, D. L. McShan, and L. Wright, *Nucl. Instrum. Methods* (to be published).
- ¹³G. D. Gunn, T. A. Schmick, L. Wright, and J. D. Fox, *Nucl. Instrum. Methods* **113**, 1 (1974).
- ¹⁴F. G. Perey, *Phys. Rev.* **131**, 745 (1963).
- ¹⁵K. A. Weber, K. Meier-Ewert, H. Schmidt-Bocking, and K. Bethge, *Nucl. Phys.* **A186**, 145 (1972).
- ¹⁶K. Bethge, C. M. Fou, and R. W. Zurmühle, *Nucl. Phys.* **A123**, 521 (1969).
- ¹⁷W. Schmidt and U. Strobbusch, *Nucl. Phys.* **A159**, 104 (1970).
- ¹⁸G. Bassani, N. Saunier, B. M. Traore, J. Raynal, A. Foti, and G. Pappalardo, *Nucl. Phys.* **A189**, 353 (1972).
- ¹⁹G. Igo, *Phys. Rev.* **115**, 1665 (1959).
- ²⁰L. A. Charlton, *Phys. Rev. C* **8**, 146 (1973); L. A. Charlton and D. Robson, Florida State University Technical Report No. 5, MERCURY (unpublished).
- ²¹V. K. Thankappan and W. W. True, *Phys. Rev.* **137**, B793 (1965).
- ²²J. L. DeJager and E. Boeker, *Nucl. Phys.* **A216**, 349 (1973).
- ²³S. Cohen and D. Kurath, *Nucl. Phys.* **A101**, 1 (1967).